Distance and Potential Dependence of Charge Transport Through the Reaction Center of Individual Photosynthetic Complexes

López-Ortiz, Manuel; Zamora, Ricardo A.; Giannotti, Marina Inés; Hu, Chen; Croce, Roberta; Gorostiza, Pau

Link to publication in VU Research Portal

Distance and Potential Dependence of Charge Transport Through the Reaction Center of Individual Photosynthetic Complexes

*Manuel López-Ortiz, Ricardo A. Zamora, Marina Inés Giannotti, Chen Hu, Roberta Croce, and Pau Gorostiza**

Charge separation and transport through the reaction center of photosystem I (PSI) is an essential part of the photosynthetic electron transport chain. A strategy is developed to immobilize and orient PSI complexes on gold electrodes allowing to probe the complex's electron acceptor side, the chlorophyll special pair P700. Electrochemical scanning tunneling microscopy (ECSTM) imaging and current–distance spectroscopy of single protein complex shows lateral size in agreement with its known dimensions, and a PSI apparent height that depends on the probe potential revealing a gating effect in protein conductance. In current–distance spectroscopy, it is observed that the distance-decay constant of the current between PSI and the ECSTM probe depends on the sample and probe electrode potentials. The longest charge exchange distance (lowest distance-decay constant β) is observed at sample potential 0 mV/SSC (SSC: reference electrode silver/silver chloride) and probe potential 400 mV/SSC. These potentials correspond to hole injection into an electronic state that is available in the absence of illumination. It is proposed that a pair of tryptophan residues located at the interface between P700 and the solution and known to support the hydrophobic recognition of the PSI redox partner plastocyanin, may have an additional role as hole exchange mediator in charge transport through PSI.

1. Introduction

Electron transfer (ET) is a charge exchange process driven by the difference in redox potential between donor and acceptor species. In biology, ET is an essential component of the electron transport chains involved in cellular respiration and photosynthesis. ET in the photosystem I (PSI) complex has been extensively studied both for basic[1] and applied purposes.[2]

PSI is a thylakoid membrane complex[3] that transfers electrons from Plastocyanin in the luminal side to Ferredoxin in the stromal side upon light exposure. This is an energetically uphill process powered by the excitonic energy harvested by the pigments found in the reaction center and in the light harvesting complex (LHCI) associated to PSI.[3,4] The combination of efficient excitonic energy transfer[4] and fast ET (10^{-8}–10^{-7} s)[5] results in a quantum yield near unit for the PSI electron transport chain. This efficiency figure of merit is often used to highlight the potential of PSI in biohybrid solar energy harvesting.[2,6,7] Upon illumination, PSI complexes are brought to a long-lived state formed by a pair of spatially and energetically distant redox cofactors: the photo-oxidized chlorophyll special pair P700+ (270 mV/SSC (SSC: reference electrode silver/silver chloride))[8] in the luminal side is an electron acceptor located 5 nm away from the terminal electron donor, the reduced iron sulfur cluster (F_b^-) in the stromal side (**Figure 1**). Thus, for illuminated PSI complexes in physiological conditions, electrons flow from P700 to F_b.

Monitoring the ET of individual redox proteins allows singling out their contribution to the ensemble current and has been enabled by in situ scanning probe techniques along with methods to specifically connect proteins to planar conductive electrodes.[9] Electrochemical scanning tunneling microscopy (ECSTM)

M. López-Ortiz, R. A. Zamora, M. I. Giannotti, P. Gorostiza
Institute for Bioengineering of Catalonia (IBEC)
The Barcelona Institute of Science and Technology
Baldiri Reixac 10–12, Barcelona 08028, Spain
E-mail: pau@icrea.cat
M. López-Ortiz, R. A. Zamora, M. I. Giannotti, P. Gorostiza
Network Biomedical Research Center on Bioengineering
Biomaterials and Nanomedicine (CIBER-BBN)
Madrid 28029, Spain

M. I. Giannotti
Department of Materials Science and Physical Chemistry
University of Barcelona
Martí i Franquès 1–11, Barcelona 08028, Spain
C. Hu, R. Croce
Biophysics of Photosynthesis
Department of Physics and Astronomy
Faculty of Sciences
Vrije Universiteit Amsterdam
De Boelelaan 1081, Amsterdam 1081 HV, The Netherlands
P. Gorostiza
Catalan Institution for Research and Advanced Studies (ICREA)
Barcelona 08010, Spain

ADVANCED
SCIENCE NEWS
www.advancedsciencenews.com

NANO · MICRO
small
www.small-journal.com

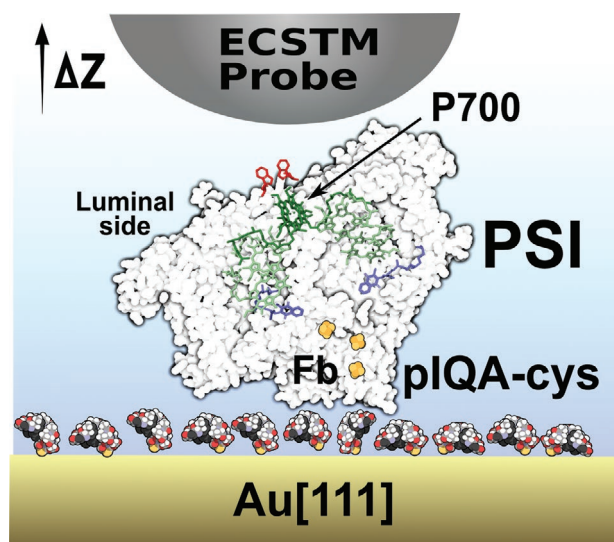**Figure 1.** Scheme of the molecular arrangement set up in this work to attach and orient PSI complexes on Au[111] atomically flat electrodes. Peptides recognizing PSI stromal side with a C-terminal cysteine residue (pIQA-cys peptide) were attached to the gold surface in order to bind plant PSI complexes. This functionalization exposes the P700 site (luminal side) to the solution, enabling reproducible bulk photoelectrochemical measurements as well as single molecule measurements like scanning probe microscopy and spectroscopy. An electrochemical scanning tunneling microscopy (ECSTM) probe electrode is depicted on top of the PSI complex (reference and auxiliary electrodes are not shown for simplicity). The electrochemical potential and position (z) of the probe can be accurately controlled during charge exchange with the P700 site.

(ECSTM) studies of several metalloproteins[9–15] have revealed a current enhancement or gating effect (see below) as the Fermi levels of the sample and probe electrodes align with the redox energy level of the protein. Alternative to ET, an electron transport (ETp) charge exchange mechanism has been proposed for protein junctions where the macromolecule contacts both electrodes. While ET is driven by redox potential, in ETp, the charge exchange is driven by the potential drop between the electrodes.[16] Although the physiological relevance of ETp through protein junctions is less studied than that of ET, understanding protein ETp is key to engineering protein-based electronic devices[16,17] as ETp has been shown[16,18–20] to be a ubiquitous charge conduction mechanism through the protein matrix of redox and non-redox proteins.[21] In particular, ETp through PSI complexes in the dark, evidenced by the current rectifying behavior of oriented PSI monolayers[22,23] is favored in the stroma-to-lumen direction (from F_b to P700) following the PSI natural dipole.[24] That is, in the dark, the preferred sense of ETp in PSI is opposite to the physiological one. As a first step to link ET and ETp in PSI, we have chosen to study the behavior of PSI under dark conditions (non-redox active state) and we have applied potentials to favor currents in the sense of PSI ETp.

We evaluate the charge exchange between PSI's P700 side and ECSTM probe by estimating the current–distance decay constant β [nm^{-1}] of the process. In ET formalism, β is proportional to the electronic coupling between donor and acceptor molecular orbitals. Experimentally, the distance decay constant β of the ET between a prosthetic ruthenium atom and the

copper center in Ru-modified Azurin (Az) mutants[25,26] yields 11 nm^{-1}. For Az functionalized in gold electrodes with alkanethiol of different lengths,[27] a value of $\beta = 1.03 \pm 0.02$ nm^{-1} per CH$_2$ is found. In an ECSTM setup, β can be directly evaluated from current–distance plots.[28] In this case, β accounts for the distance decay resulting from all charge exchange processes between the protein-functionalized sample and probe electrodes. For instance, the β value for bare gold electrodes in physiological medium is 10 nm^{-1}. In gold electrodes functionalized with Az proteins,[28] β is 4 nm^{-1} and similar β values have been obtained for DNA base pairs[29] and redox proteins.[30,31] Moreover, β is modulated by the electrode potential and it is lowest (i.e., the spatial span of the current is longest) for electrode potentials matching the redox level of the protein[28,30,31] or redox-active organic compound.[32] Our previous results with PSI complexes[30] suggest that long-distance charge transport is electrochemically gated.[30] In that work, we used thiolated self-assembled monolayers (SAM) exposing a negatively charged surface, which have been largely employed for PSI immobilization.[33] The present study aims to determine the distance and potential dependence of ET/ETp through the P700 reaction center of PSI and thus requires better defined protein orientation, and higher recognition specificity.

A preferential yet heterogeneous orientation of PSI molecules is obtained with SAM-PSI electrostatic interactions.[33] PSI orientation can be inferred from the current-rectifying behavior of SAM-PSI monolayers evaluated with STM[34] and C-AFM.[22] Specific binding and orientation of cyanobacterial PSI complexes to indium tin oxide (ITO) electrodes has been achieved with a synthetic peptide (pIQA)[23] that binds to the stromal side of cyanobacterial PSI from *Thermosynechococcus elongatus*. PSI orientation was evaluated from the current-rectifying behavior of the PSI-pIQA-ITO monolayer. To investigate the charge exchange process with the P700 site in PSI, here we have designed a pIQA derivative to bind and orient plant PSI complexes on atomically flat gold electrodes. We reasoned that the pIQA structure would be recognized by the plant PSI based on the sequence similarity between the PSI stromal side regions from cyanobacterial PSI and plant PSI (see Supporting Information and Figures S1–S4, Supporting Information). We modified the pIQA peptide for Au substrate attachment by introducing a cysteine (pIQA-cys).[23] The resulting PSI-pIQA-cys-Au functionalization yields robust macroscopic photocurrents in a wide potential window and enables reproducible high-resolution microscopy and spectroscopy of individual PSI complexes. In these conditions, the charge exchange between the P700 site exposed to the solution and the ECSTM probe reveals long distance dependence (low β value) and electrochemical gating. The results are in agreement with hole injection into PSI and reveal the presence of a low-energy state in the absence of illumination.

2. Results and Discussion

Topography of oriented PSI on Au by using atomic force microscopy (AFM) of PSI-pIQA-cys-Au electrodes (**Figure 2**a–c) shows the presence of a homogeneous and partial electrode surface coverage of 6 nm thickness, which is in agreement with previously reported PSI assemblies on gold[35,36] (see Supporting
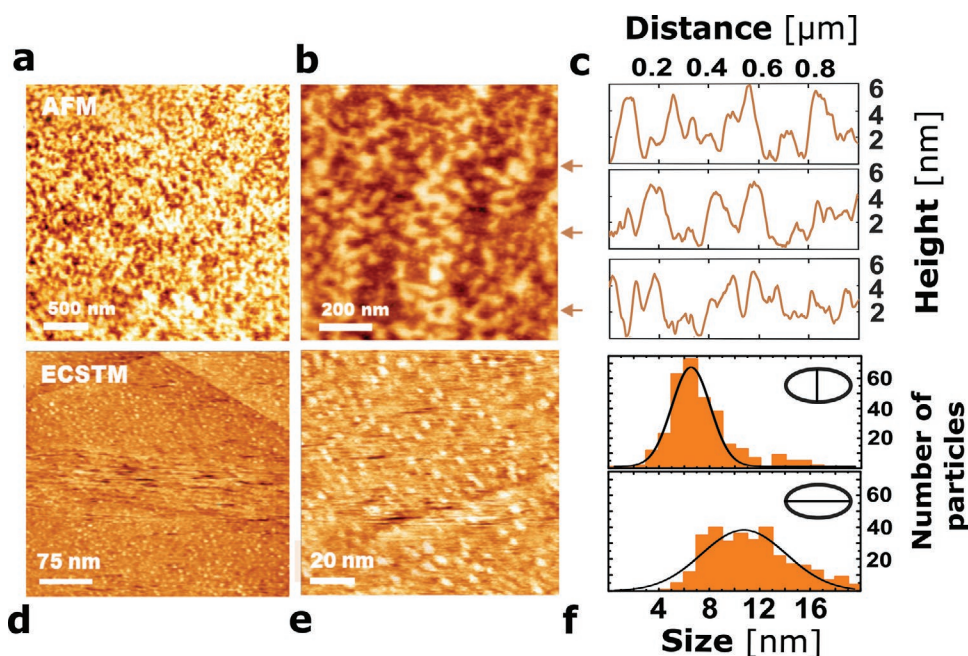
**ADVANCED
SCIENCE NEWS**
www.advancedsciencenews.com

**NANO · MICRO
small**
www.small-journal.com

Figure 2. Structural characterization of of PSI-pIQA-cys-Au films attached to atomically flat Au[111] electrodes. AFM image of PSI-pIQA-cys-Au, a) scan size 3×3 μm and b) 1×1 μm. The vertical (z) color scale is set to 8 nm amplitude. c) Example AFM height profiles at the positions indicated with arrows in panel (b). ECSTM images of the same sample, d) 350×350 nm and e) 150×150 nm. The vertical (z) color scales correspond to 1.4 and 1.1 nm, respectively. The set point tunnel current is 0.2 nA and the bias is 300 mV ($U_S = 0$ mV/SSC, $U_P = 300$ mV/SSC). f) Distribution of ECSTM particle size, short axis (top), and long axis (bottom).

Information and Figure S5, Supporting Information). The lateral size of PSI single particles was not determined due to limited AFM probe resolution. Single complex resolution is achieved in ECSTM image (Figure 2d,e). For each complex, long and short axes in the horizontal plane were fit with a 2D-gaussian model (Figure S6, Supporting Information). Size distribution for $N = 334$ particles yields 6.5 ± 0.1 nm and 10.7 ± 0.3 nm for short and long axes respectively. Protein lateral sizes, taken as full width at half maximum, are 60% and 70% smaller than available crystallographic structure of PSI-LHCI structure,[37] with approximate sizes of 10.5 and 15 nm, respectively.

The topography (apparent height) of PSI-pIQA-cys-Au samples observed by ECTSM (**Figure 3**a) is tenfold lower than that observed by AFM (Figure 2a,b). This result agrees with previous reports about PSI complexes on alkanethiol-functionalized gold substrates.[30] Since ECSTM is operated in constant current feedback mode, the apparent height is due both to the topography and to the conductance of the sample. ECSTM apparent heights lower than the known structural dimensions have been observed for several proteins deposited on metal substrates.[27,38–42] These results confirm that protein conductance is larger than that of
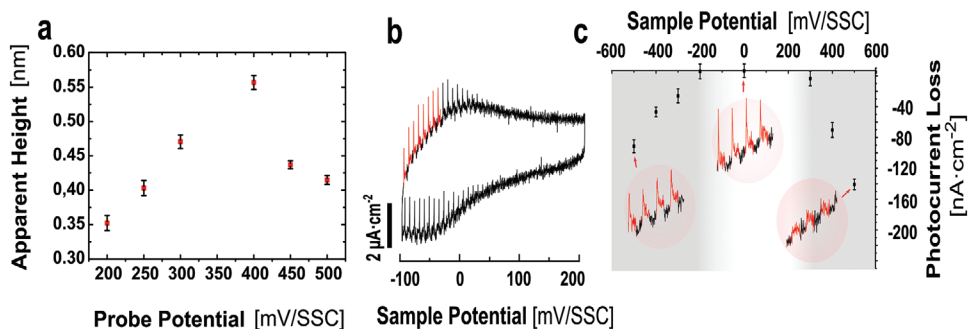

Figure 3. Dependence of PSI-pIQA-cys-Au microscopy and photocurrent recordings on the electrochemical potential: a) Apparent height of PSI complexes measured from ECSTM image profiles at different probe potentials U_P (constant bias potential $U_{bias} = U_P - U_S = 300$ mV/SSC). A maximum PSI height is observed at $U_P = 400$ mV/SSC indicating a conductance resonance as observed for redox proteins and complexes. b) Bulk photoelectrochemical current measured in a PSI-pIQA-cys-Au sample during cyclic voltammetry at 80 mV s^{-1} rate while switching on and off the 690 nm illumination every 125 ms (red and black traces, respectively). Photoresponses are observed at $U_S < 100$ mV/SSC. c) An electrochemical potential window of PSI stability between −200 and +300 mV/SSC is identified where photocurrent loss is below 10% (white band and example photocurrent recording at the center, red traces corresponding to 690 nm illumination). Applying potentials outside this window diminishes photoresponses (indicated by grey bands and example photocurrent traces).

**ADVANCED
SCIENCE NEWS**

www.advancedsciencenews.com

NANO · MICRO

small

www.small-journal.com

the surrounding electrolytic medium, both in metalloproteins[43–45] and interestingly, in non-redox active proteins.[18,19] In addition, we observe that the apparent height of PSI complexes by ECSTM depends on the probe potential U_P (Figure 3a). This effect allows using ECSTM imaging at different electrochemical potentials to study their conductance and charge transport properties. Several works showed a similar dependence in the small globular protein Az,[12,13] and more recently, in a 100 kDa oxidoreductase complex.[46] This gated conductance resonance is attributed to the alignment of the Fermi levels of the ECSTM sample and probe electrodes with the redox energy (molecular orbital) of the molecule under study.

To define a working electrochemical window, chopped light cyclic voltammetry (CV) experiments (Figures S7, S8, and S9, Supporting Information) were performed. Soluble redox mediators methyl viologen (125 μM) and osmium bipyridine dichloride (10 μM) were added to the buffer solution to enhance photocurrents and facilitate the characterization.[36] Illuminating PSI complexes at $U_S = -100$ mV/SSC produces photocurrents with 1 μA·cm^{-2} transient and 200 nA·cm^{-2} steady components (Figure 3b; Figure S8, Supporting Information) while no photocurrents are observed in the absence of PSI (Figure S7, Supporting Information). Photocurrents depend on the applied sample potential and can only be measured below 100 mV/SSC. Potential excursions within the range −200 mV/SSC to 300 mV/SCC do not alter the magnitude of photocurrents, but they are reduced after applying potentials outside this "safe" electrochemical window (Figures S8 and S9, Supporting Information). The photocurrent loss (Figure 3c) was estimated comparing photocurrents measured in a reference potential region between −100 mV/SSC and −25 mV/SSC (indicated by red traces in Figure 3b) before and after applying a test potential during 5 min (Figures S8 and S9, Supporting Information). For potentials $U_S < -200$ mV/SSC, cathodic currents increase significantly due to the presence of O_2 in the electrochemical cell.[47–49] After applying $U_S = -400$ mV/SSC for 5 min (Figure S8, Supporting Information), the voltammogram is broadened indicating a decrease of the electrode capacity revealing a partial depletion of absorbed molecules while a decrease in photocurrent amplitude is also observed. Photocurrent degradation has been attributed to the formation of ROS in aerobic systems where O_2 acts as terminal electron acceptor.[47,48] Similar irreversible decrease of photocurrent and electrode capacity is observed for positive potentials ($U_S > 300$ mV/SSC) that could be associated to the desorption of molecules absorbed on the electrode. The appearance of an anodic peak at 500 mV/SSC (Figure S8, Supporting Information) in PSI-pIQA-cys-Au samples that is not present in pIQA-cys samples and the stability pIQA-cys-Au samples (red traces in Figure S7, Supporting Information) suggest that the decrease in photocurrent observed in Figure 3c could be attributed to PSI desorption.

Reversible and stable photocurrent measurements in the electrochemical window between −200 mV/SSC < U_S < +300 mV/SSC indicate the presence of functional (photoactive) PSI complexes in the electrode. We took these values to set the sample potential boundaries to study single PSI spectroscopy with ECSTM in the dark. Thus, in Figures 2 and 3,

the microscopic and bulk photocurrent characterization of pIQA-cys peptide functionalized gold electrodes show: (i) functionalization of PSI complexes on Au electrodes modified with a cysteine peptide, (ii) conductance gating in the PSI apparent height measured by ECSTM, as reported for other proteins and complexes, (iii) bulk photocurrent measurements demonstrate that PSI complexes remain (photo)active upon attachment to the electrode, and (iv) a safe working electrochemical window is identified where PSI activity is retained. Finally, the activity of PSI-pIQA-cys-Au samples was tested with photo–chrono–amperometry, in the absence of redox mediators, before current decay spectroscopy experiments, acquiring photocurrents of 10 nA·cm^{-2} at $U_S = -100$ mV/SSC (Figure S10, Supporting Information) while no photocurrents were observed in the absence of PSI complexes. These results set the stage for reproducible ECSTM current–distance decay experiments in the next section.

We used ECSTM to evaluate the distance decay constant of currents in PSI-pIQA-cys-Au samples at fixed locations. The charge exchange process between sample and probe electrodes was measured in dark conditions to prevent photo-oxidation of the P700 site[28] (i.e., in the absence of redox activity of PSI). ECSTM spectroscopy recordings were performed as previously described.[28] Briefly, we departed from a set-point current of 300 pA and switched off the feedback control loop prior to retracting the probe electrode (a Pt–Ir sharp tip) away from the sample electrode (an Au[111] monocrystal, see Supporting Information) at a constant rate, while measuring the probe current. Current–distance spectra were recorded under bi-potentiostatic control of probe and sample. We set 11 pairs of potentials for the sample ($U_s = -100$, 0, 100, and 200 mV/SSC) and probe ($U_p = 200$, 300, and 400 mV/SSC) which yield applied bias ranging from +100 to +500 mV ($U_{bias} = U_P - U_S$). The positive sign in bias potential was chosen to follow the favored sense of ETp for PSI in dark from stroma to lumen.[22,23] Logarithmic current plots (**Figure 4**a) for PSI-pIQA-cys-Au (blue) show longer charge exchange distance with respect to pIQA-cys-Au controls (black). While most control traces are well described by a single exponential decay model, PSI data shows a double exponential behavior (Figure S11, Supporting Information). Double exponential traces exhibit a short distance regime with $z < 0.2$ nm (Figure S12, Supporting Information) and a second regime spanning from 0.2 nm to 1.0–2.5 nm depending on the applied probe potential. Beyond 2.5 nm, the probe current is masked by faradaic currents (≈25 pA) due to probe insulation defects. Double exponential behavior has already been reported for DNA molecules[29] and proteins[30,31] and has been attributed to the surface charge screening.[28]

In the absence of PSI, the distribution of β values is centered around 7 nm^{-1} and is independent of potential. In contrast, the β values for PSI-pIQA-cys-Au depends both on the sample and probe potentials. At sample potentials above 100 mV/SSC, β is ≈4–5 nm^{-1}, similar to previously reported values for Az[28] and PSI complexes.[30] However, at sample potentials equal or below 0 mV/SSC and probe potential 400 mV/SSC, we obtained β values below 2 nm^{-1}, which cannot be accounted for by a tunneling mechanism and are reminiscent of the long-distance currents observed for Cc–bc_1.[31]

ADVANCED
SCIENCE NEWS
www.advancedsciencenews.com

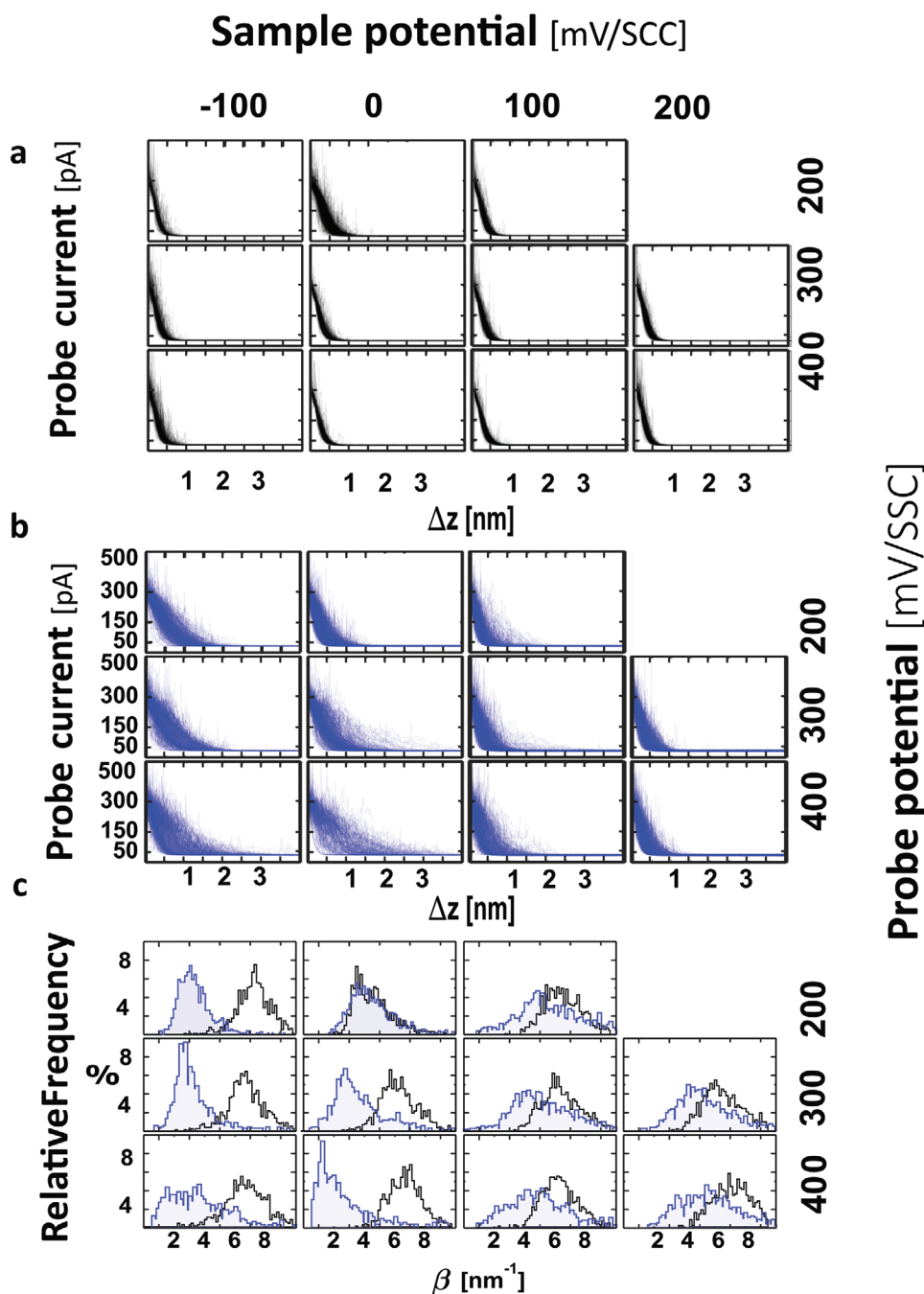NANO · MICRO
small
www.small-journal.com

Figure 4. Electrochemical current–distance spectroscopy measurements with ECSTM at different sample and probe potentials: a) Semilogarithmic plots of I(z) recordings of pIQA-cys-Au samples (black) and b) PSI-pIQA-cys-Au (blue) at U_S potentials within the safe window for PSI activity and at U_P potentials to probe charge exchange with PSI using moderate bias values. Long distance decay is observed around $U_S = 0$ mV/SSC and $U_P = 400$ mV/SSC. c) Normalized distribution of β distance-decay constant obtained for each condition in panels (a,b). Low values of β (≈ 1 nm^{-1}) are observed at $U_S = 0$, $U_P = 400$ mV/SSC.

The effect of sample and probe potentials on β values distribution (see Figure S13, Supporting Information) is shown, respectively, in **Figure 5**a,b. We remark that β values below 4 nm^{-1} are only found for $U_S < 100$ mV/SSC irrespective of the applied probe potential. Thus, applying a sample potential $U_S < 100$ mV/SSC is a necessary condition for enhanced charge exchange distance in the dark. Interestingly, bulk photoelectrochemical currents are only observed below this potential (Figure 3b). Fulfilling this condition ($U_S < 100$ mV/SSC), β value decreases as the probe potential is increased (Figure 5b). The lowest β values (longest charge exchange distances) are found at $U_P = 400$ mV/SSC and bias potentials $U_{bias} = 500$ mV ($U_S = 0$ mV/SSC) and $U_{bias} = 400$ mV ($U_S = 0$ mV/SSC). These results suggest that farthest-reaching currents are due to the probe potential (Fermi energy
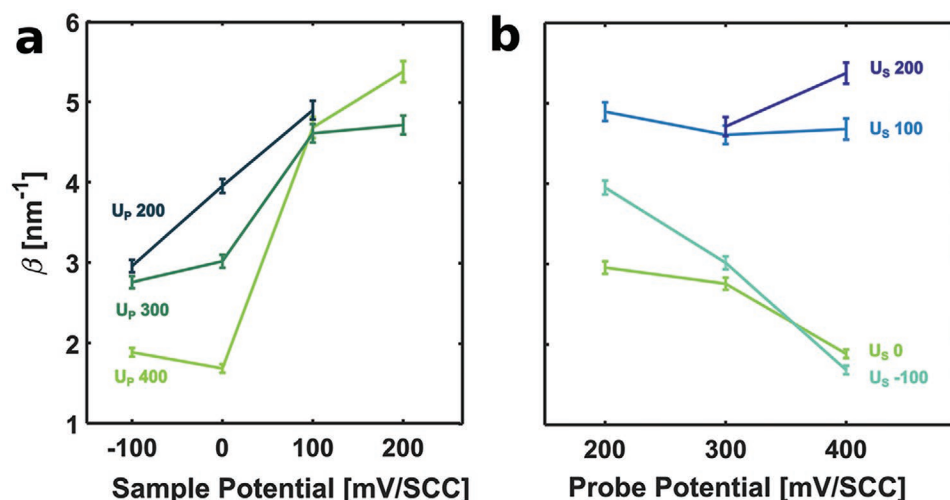
Figure 5. Dependence of the distance decay constant β of PSI-pIQA-cys-Au with the electrochemical potentials. The plots show the statistical representation of β values obtained from Figure 4c. a) β values vs applied sample potential. Probe potentials are indicated in color (U_P = 200, 300, 400 mV/SSC for blue, light green, and dark green traces, respectively). b) β values vs applied probe potential with sample potential traces (U_S = 200, 100, 0, and −100 mV/SSC) represented in dark blue, light blue, green, and aquamarine respectively. The lowest values (corresponding to the farthest-reaching currents) are observed at U_S = 0 mV/SSC and U_P = 400 mV/SSC.

position ≈ −5.0 eV versus the vacuum level) irrespectively of the applied bias (driving force). The β values as a function of sample and probe electrodes are summarized in **Figure 6**.

It has been reported that β values in redox proteins[28,30,31] and organic compounds[32] depend on the electrode potentials. In PSI-pIQA-cys-Au, β values depend on the probe rather than on the sample potential (provided that U_s < −100 mV/SSC). We argue that the electric potential at the luminal side of PSI complexes is set by the probe electrode facing the P700 side while the sample potential is screened by pIQA-cys peptide and the 5 nm thick PSI protein matrix. In this sense, the probe electrode can be likened to a PSI redox partner under potentiostatic control.

In these experiments, we have focused on ETp through PSI bound to the sample electrode via pIQA-cys peptide and we have avoided ET (redox) effects like direct oxidation of P700 site by carrying out current–distance recordings in dark conditions. However, in contrast to ETp measurements, no direct molecular bond is established between the luminal side of PSI and the ECSTM probe and thus, current flow depends to some extent on the aqueous solution, which may involve water molecules and protons as it occurs in ET. This partial electronic decoupling between the electrode and PSI can be seen as an advantage of ECSTM that enabled us to observe gating effects in imaging and spectroscopic experiments of PSI (Figures 3 and 4), as previously found for cytochrome c and Az. It might allow studying the role of electronic coupling between PSI and its partners in the overall photosynthetic electron transport chain.

We reasoned that the dependence of β on U_P (Figure 6) could be due to the presence of a cofactor or residue on the luminal surface whose molecular orbital could be electronically coupled to the ECSTM probe at 400 mV/SSC (low electron energies). We thus examined the residues on the luminal surface of PSI that could mediate this process, and noticed a pair of

tryptophan residues (Trp625 and Trp658 in Figure 6d)[37] that is located in the proximity of P700 and integrates the hydrophobic recognition site of plastocyanin (Pc), an electron donor partner protein of PSI.[50–52] Tryptophan is an oxidizable aromatic residue whose redox activity is involved in photosynthetic water splitting, nucleic acid biosynthesis, and cell signaling, acting as a hole carrier. It plays a major role in proton-coupled electron transfer,[53,54] and mediates photoinduced long-range ET in photolyase[55,56] and in dye-modified Az mutants.[57,58] In plants cryptochrome, the ET rate is modified by two orders of magnitude by ATP binding and by pH modulating the electronic coupling of a Trp residue.[59]

Regarding protein–electrode interfaces, it has been proposed that charge exchange is modulated by electronic coupling between electrode Fermi level and the molecular orbitals of interfacing residues.[18,20,21,43,44,60,61] Remarkably, introducing Trp residues in 6-Alanine peptides increases their molecular conductance, lowering the effective barrier height and enhancing electronic coupling with gold electrodes.[62] In addition, cyclic voltammetry features of Az are abolished if the Trp residue mediating ETp with the electrode is mutated.[63] All these results suggest that aromatic Trp residues play a significant role in protein ET and in ETp. Based on our current–distance spectroscopy results, we hypothesize that surface exposed Trp625 and Trp658 may act as primary electron donors (hole acceptors) to the ECSTM probe, which would explain the gating of the apparent height and β.

The physiological role of Trp residues has been studied in PSI and transient absorption experiments demonstrated that the ET kinetics of PSI with Pc are altered in *Chlamydomonas reinhardtii* mutants Trp627Phe and Trp651Ser[64,65] (corresponding to Trp625 and Trp658 in *Arabidopsis thaliana* respectively). In bulk transient absorption measurements, the kinetic contribution of the formation of a productive complex, reorganization, ET, and unbinding processes is indirectly inferred from the
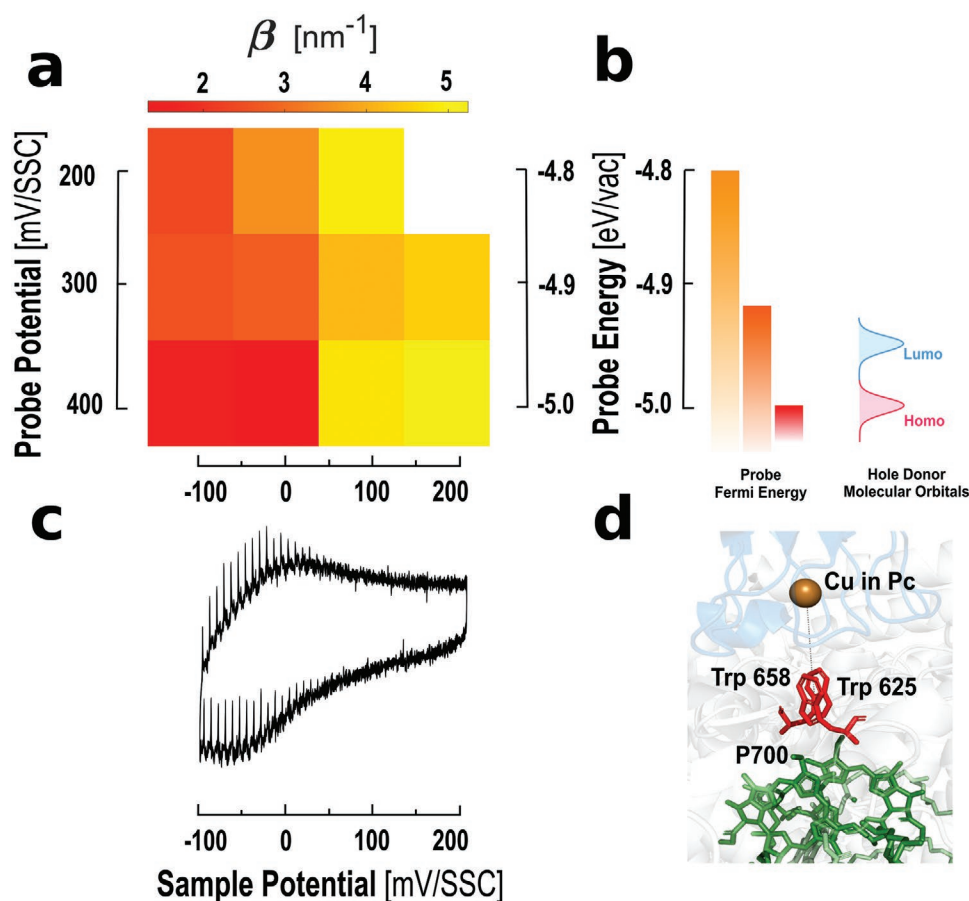
ADVANCED
SCIENCE NEWS
www.advancedsciencenews.com

NANO · MICRO
small
www.small-journal.com

Figure 6. Diagram of distance-decay rates of PSI-pIAS-cys-Au showing electrochemically gated long distance current between the ECSTM probe and the P700 site of PSI in the dark. a) Distance decay constant β average values are plotted in color scale (red corresponding to 2 nm^{-1} and yellow to 5 nm^{-1}) as a function of the probe and sample potentials and using the same layout as Figure 4. b) The correspondence of the vertical axis with the electron energy of the probe is shown in the scale on the right, together with a diagram depicting hole injection from the probe at $U_P = 400$ mV/SSC into a hypothetic electron donor state of PSI in the dark. c) A chopped light voltammogram (Figure 3) is indicated under the horizontal axis to show the sample potential range of PSI photo-responses. d) Candidate electron donor sites that could mediate this current include a pair of oxidizable tryptophan residues (Trp625, Trp658, shown in red) located between P700 (green) and the copper active site of the PSI redox partner plastocyanin (Pc, orange).

different time components of the transient absorption signal. In contrast, distance- and potential-dependent ECSTM experiments allow evaluating the independent contribution of the ET process to the overall charge transport process. Our results suggest that these Trp residues play an additional role as hole exchange mediators in PSI, possibly regulating ET through electronic coupling, in line with findings in other protein systems.

3. Conclusion

In summary, we have developed a strategy to functionalize gold electrodes with plant PSI complexes that orients and exposes their luminal side to the electrolyte, in order to investigate charge exchange processes mediated by their P700 site. Sample preparation is based on a peptide sequence that binds specifically to the stromal side of PSI from cyanobacteria and plants and it should be applicable to a variety of complexes and substrates. Bulk photoelectrochemical measurements demonstrate

that PSI complexes remain fully functional in a wide window around 0 mV/SSC sample potential. Nanoscale imaging of individual complexes shows lateral sizes in agreement with the dimensions of PSI and an apparent height that is electrochemically gated for ECSTM probe potentials around 400 mV/SSC. This experimental setup enables for the first time, spectroscopic measurements with ECSTM (current–distance decay at different electrochemical potentials) that unequivocally correspond to the P700 side of PSI exposed to the aqueous medium. In these conditions, we observe that the spatial span of the current is enhanced (the distance-decay constant β is reduced) through the solution at sample potential 0 mV/SSC and probe potential 400 mV/SSC. This process corresponds to hole injection into an electronic state that is available in the absence of illumination. We propose that a pair of tryptophan residues (Trp625, Trp658) located near P700 and known to integrate the hydrophobic recognition site for Pc may have an additional role as hole exchange mediator involved in the charge transport process through PSI.

Supporting Information

Supporting Information is available from the Wiley Online Library or from the author.

Acknowledgements

Conflict of Interest

The authors declare no conflict of interest.

Data Availability Statement

The data that support the findings of this study are openly available in chemRxiv at https://doi.org/10.26434/chemrxiv.14556048.v1, reference number1026434.

Keywords

[1] K. Brettel, *Biochim. Biophys. Acta, Bioenerg.* **1997**, *1318*, 322.
[2] A. H. Teodor, B. D. Bruce, *Trends Biotechnol.* **2020**, *38*, 1329.
[3] J. H. Golbeck, *Photosystem I: The Light-Driven Plastocyanin:Ferredoxin Oxidoreductase*, Advances in Photosynthesis and Respiration, Vol. *24*, **2010**.
[4] R. Croce, H. van Amerongen, *Science* **2020**, *369*, eaay2058.
[5] P. R. Chitnis, *Annu. Rev. Plant Physiol. Plant Mol. Biol.* **2001**, *52*, 593.
[6] X. Qiu, O. Castañeda, E. Ocampo, H. W. de Vries, M. van Putten, M. Loznik, A. Herrmann, R. C. Chiechi, *ACS Appl. Mater. Interfaces* **2018**, *10*, 37625.
[7] N. Nelson, *J. Nanosci. Nanotechnol.* **2009**, *9*, 1709.
[8] A. Nakamura, T. Suzawa, Y. Kato, T. Watanabe, *Plant Cell Physiol.* **2011**, *52*, 815.
[9] P. Salvatore, D. Zeng, K. K. Karlsen, Q. Chi, J. Wengel, J. Ulstrup, *ChemPhysChem* **2013**, *14*, 2101.
[10] J. Zhang, A. M. Kuznetsov, J. Ulstrup, *J. Electroanal. Chem.* **2003**, *541*, 133.
[11] J. Zhang, Q. Chi, A. M. Kuznetsov, A. G. Hansen, H. Wackerbarth, H. E. M. Christensen, J. E. T. Andersen, J. Ulstrup, *J. Phys. Chem. B* **2002**, *106*, 1131.
[12] A. Alessandrini, S. Corni, P. Facci, *Phys. Chem. Chem. Phys.* **2006**, *8*, 4383.
[13] Q. Chi, O. Farver, J. Ulstrup, *Proc. Natl. Acad. Sci. USA* **2005**, *102*, 16203.
[14] J. M. Artés, M. López-Martínez, I. Díez-Pérez, F. Sanz, P. Gorostiza, *Small* **2014**, *10*, 2537.
[15] M. López-Martínez, J. M. Artés, V. Sarasso, M. Carminati, I. Díez-Pérez, F. Sanz, P. Gorostiza, *Small* **2017**, *13*, 1700958.
[16] C. D. Bostick, S. Mukhopadhyay, M. Sheves, D. Cahen, D. Lederman, *Rep. Prog. Phys.* **2018**, *81*, 026601.
[17] J. M. Artés, I. Díez-Pérez, P. Gorostiza, *Nano Lett.* **2012**, *12*, 2679.
[18] B. Zhang, W. Song, J. Brown, R. Nemanich, S. Lindsay, *J. Am. Chem. Soc.* **2020**, *142*, 6432.
[19] B. Zhang, W. Song, P. Pang, H. Lai, Q. Chen, P. Zhang, S. Lindsay, *Proc. Natl. Acad. Sci. U.S.A.* **2019**, *116*, 5886.
[20] I. Ron, L. Sepunaru, S. Ltzhakov, T. Belenkova, N. Friedman, I. Pecht, M. Sheves, D. Cahen, *J. Am. Chem. Soc.* **2010**, *132*, 4131.
[21] S. Lindsay, *Life* **2020**, *10*, 72.
[22] O. E. Castañeda Ocampo, P. Gordiichuk, S. Catarci, D. A. Gautier, A. Herrmann, R. C. Chiechi, *J. Am. Chem. Soc.* **2015**, *137*, 8419.
[23] P. Gordiichuk, D. Pesce, O. E. C. Ocampo, A. Marcozzi, G.-J. A. H. Wetzelaer, A. Paul, M. Loznik, E. Gloukhikh, S. Richter, R. C. Chiechi, A. Herrmann, *Adv. Sci.* **2017**, *4*, 1600393.
[24] B. van Haeringen, J. P. Dekker, M. Bloemendal, M. Rögner, R. van Grondelle, H. van Amerongen, *Biophys. J.* **1994**, *67*, 411.
[25] R. Langen, I. J. Chang, J. P. Germanas, J. H. Richards, J. R. Winkler, H. B. Gray, *Science* **1995**, *268*, 1733.
[26] J. R. Winkler, H. B. Gray, *Chem. Rev.* **2014**, *114*, 3369.
[27] Q. Chi, J. Zhang, J. E. T. Andersen, J. Ulstrup, *J. Phys. Chem. B* **2001**, *105*, 4669.
[28] J. M. Artés, I. Díez-Pérez, F. Sanz, P. Gorostiza, *ACS Nano* **2011**, *5*, 2060.
[29] J. He, L. Lin, P. Zhang, S. Lindsay, *Nano Lett.* **2007**, *7*, 3854.
[30] M. López-Martínez, M. López-Ortiz, M. E. Antinori, E. Wientjes, A. Nin-Hill, C. Rovira, R. Croce, I. Díez-Pérez, P. Gorostiza, *Angew. Chem., Int. Ed.* **2019**, *58*, 13280.
[31] A. Lagunas, A. Guerra-Castellano, A. Nin-Hill, I. Díaz-Moreno, M. A. de la Rosa, J. Samitier, C. Rovira, P. Gorostiza, *Nat. Commun.* **2018**, *9*, 3.
[32] D. I. Gittins, D. Bethell, D. J. Schiffrin, R. J. Nichols, *Nature* **2000**, *408*, 67.
[33] G. Leblanc, E. Gizzie, S. Yang, D. E. Cliffel, G. K. Jennings, *Langmuir* **2014**, *30*, 10990.
[34] I. Lee, J. W. Lee, E. Greenbaum, *Phys. Rev. Lett.* **1997**, *79*, 3294.
[35] D. Mukherjee, M. May, M. Vaughn, B. D. Bruce, B. Khomami, *Langmuir* **2010**, *26*, 16048.
[36] A. K. Manocchi, D. R. Baker, S. S. Pendley, K. Nguyen, M. M. Hurley, B. D. Bruce, J. J. Sumner, C. A. Lundgren, *Langmuir* **2013**, *29*, 2412.
[37] X. Qin, M. Suga, T. Kuang, J. R. Shen, *Science* **2015**, *348*, 989.
[38] D. Alliata, L. Andolfi, S. Cannistraro, *Ultramicroscopy* **2004**, *101*, 231.
[39] L. Andolfi, G. W. Canters, M. P. Verbeet, S. Cannistraro, *Biophys. Chem.* **2004**, *107*, 107.
[40] L. Andolfi, B. Bonanni, G. W. Canters, M. P. Verbeet, S. Cannistraro, *Surf. Sci.* **2003**, *530*, 181.
[41] J. Zhang, Q. Chi, J. U. Nielsen, E. P. Friis, J. E. T. Andersen, J. Ulstrup, *Langmuir* **2000**, *16*, 7229.
[42] J. Zhang, H. E. M. Christensen, B. L. Ooi, J. Ulstrup, *Langmuir* **2004**, *20*, 10200.
[43] K. Garg, M. Ghosh, T. Eliash, J. H. van Wonderen, J. N. Butt, L. Shi, X. Jiang, F. Zdenek, J. Blumberger, I. Pecht, M. Sheves, D. Cahen, *Chem. Sci.* **2018**, *9*, 7304.
[44] Z. Futera, I. Ide, B. Kayser, K. Garg, X. Jiang, J. H. van Wonderen, J. N. Butt, H. Ishii, I. Pecht, M. Sheves, D. Cahen, J. Blumberger, *J. Phys. Chem. Lett.* **2020**, *11*, 9766.

**ADVANCED
SCIENCE NEWS**

www.advancedsciencenews.com

NANO · MICRO

small

www.small-journal.com

[45] C. Baldacchini, A. R. Bizzarri, S. Cannistraro, *Eur. Polym. J.* **2016**, *83*, 407.

[46] J. Yan, E. E. Frøkjær, C. Engelbrekt, S. Leimkühler, J. Ulstrup, U. Wollenberger, X. Xiao, J. Zhang, *ChemElectroChem* **2021**, *8*, 164.

[47] J. Yan, E. E. Frøkjær, C. Engelbrekt, S. Leimkühler, J. Ulstrup, U. Wollenberger, X. Xiao, J Zhang, *ChemElectroChem* **2021**, *8*, 164.

[48] F. Zhao, A. Ruff, M. Rögner, W. Schuhmann, F. Conzuelo, *J. Am. Chem. Soc.* **2019**, *141*, 5102.

[49] T. Bennett, H. Niroomand, R. Pamu, I. Ivanov, D. Mukherjee, B. Khomami, *Phys. Chem. Chem. Phys.* **2016**, *18*, 8512.

[50] M. Hervás, J. A. Navarro, B. de La Cerda, A. Díaz, M. A. de La Rosa, *Bioelectrochem. Bioenerg.* **1997**, *42*, 249.

[51] T. Ueda, N. Nomoto, M. Koga, H. Ogasa, Y. Ogawa, M. Matsumoto, P. Stampoulis, K. Sode, H. Terasawa, I. Shimadaa, *Plant Cell* **2012**, *24*, 4173.

[52] A. B. Hope, *Biochim. Biophys. Acta, Bioenerg.* **2000**, *1456*, 5.

[53] A. Migliore, N. F. Polizzi, M. J. Therien, D. N. Beratan, *Chem. Rev.* **2014**, *114*, 3381.

[54] E. F. Yee, B. Dzikovski, B. R. Crane, *J. Am. Chem. Soc.* **2019**, *141*, 17571.

[55] F. Cailliez, P. Müller, T. Firmino, P. Pernot, A. de La Lande, *J. Am. Chem. Soc.* **2016**, *138*, 1904.

[56] R. Martin, F. Lacombat, A. Espagne, N. Dozova, P. Plaza, J. Yamamoto, P. Müller, K. Brettel, A. de La Lande, *Phys. Chem. Chem. Phys.* **2017**, *19*, 24493.

[57] C. Shih, A. K. Museth, M. Abrahamsson, A. M. Blanco-Rodriguez, A. J. di Bilio, J. Sudhamsu, B. R. Crane, K. L. Ronayne, M. Towrie, A. Vlček, J. H. Richards, J. R. Winkler, H. B. Gray, *Science* **2008**, *320*, 1760.

[58] K. Takematsu, H. R. Williamson, P. Nikolovski, J. T. Kaiser, Y. Sheng, P. Pospíšil, M. Towrie, J. Heyda, D. Hollas, S. Záliš, H. B. Gray, A. Vlček, J. R. Winkler, *ACS Cent. Sci.* **2019**, *5*, 192.

[59] F. Cailliez, P. Mu, M. Gallois, A. de la Lande, *J. Am. Chem. Soc.* **2014**, *136*, 12974.

[60] J. A. Fereiro, G. Porat, T. Bendikov, I. Pecht, M. Sheves, D. Cahen, *J. Am. Chem. Soc.* **2018**, *140*, 13317.

[61] X. Yu, R. Lovrincic, L. Sepunaru, W. Li, A. Vilan, I. Pecht, M. Sheves, D. Cahen, *ACS Nano* **2015**, *9*, 9955.

[62] C. Guo, X. Yu, S. Refaely-Abramson, L. Sepunaru, T. Bendikov, I. Pecht, L. Kronik, A. Vilan, M. Sheves, D. Cahen, *Proc. Natl. Acad. Sci. U.S.A.* **2016**, *113*, 10785.

[63] K. Fujita, N. Nakamura, H. Ohno, B. S. Leigh, K. Niki, H. B. Gray, J. H. Richards, *J. Am. Chem. Soc.* **2004**, *126*, 13954.

[64] F. Sommer, F. Drepper, M. Hippler, *J. Biol. Chem.* **2002**, *277*, 6573.

[65] F. Sommer, F. Drepper, W. Haehnell, M. Hippler, *J. Biol. Chem.* **2004**, *279*, 20009.